

CCD Photometry of the Globular Cluster NGC 5986 and its Post-Asymptotic-Giant-Branch and RR Lyrae Stars

David R. Alves, Howard E. Bond¹,

Space Telescope Science Institute, 3700 San Martin Dr., Baltimore, MD 21218;
 alves, bond@stsci.edu

Christopher Onken²

Department of Astronomy, University of Minnesota, 116 Church Street SE, Minneapolis,
 MN 55455; onken@sps.spa.umn.edu

ABSTRACT

We have obtained new CCD BV photometry of the little-studied southern Galactic globular cluster NGC 5986, including light curves of 5 of its RR Lyrae variables. The cluster's red giant branch bump is detected for the first time at $V = 16.47 \pm 0.03$. We derive a reddening and true distance modulus of $E(B - V) = 0.29 \pm 0.02$ and $(m - M)_0 = 15.15 \pm 0.10$, respectively. The cluster's color-magnitude diagram reveals a mostly blue horizontal branch, like that of M13 or M2, and quite unlike M3; yet all of these clusters have nearly identical metallicities ($[\text{Fe}/\text{H}]_{CG97} = -1.35$). We show that the RR Lyrae variables in NGC 5986 are about 0.2 mag brighter on average than those in M3, an important exception to the often-employed, universal $M_V(\text{RR}) - [\text{Fe}/\text{H}]$ relation. Finally, we note that NGC 5986 contains two luminous stars with spectral types A-F, which are likely to be post-asymptotic-giant-branch (PAGB) objects. The V -band luminosity function (LF) of such yellow PAGB stars is a promising standard candle. We suggest that the LF is sharply peaked at $M_V(\text{PAGB}) = -3.28 \pm 0.07$.

¹Guest observer at Cerro Tololo Inter-American Observatory, National Optical Astronomy Observatories, operated by AURA under contract with NSF.

²1999 summer student at the Space Telescope Science Institute. Now affiliated with the Department of Astronomy, The Ohio State University.

1. Introduction

Population II stars evolving off the asymptotic giant branch (AGB) and passing through spectral types F and A are excellent candidates for a new extragalactic standard candle (Bond 1997, 2001). These “yellow” post-AGB (PAGB) stars are the visually brightest members of old populations. They should have a narrow luminosity function (LF), because essentially a single main-sequence turnoff mass is feeding the PAGB region of the HR diagram. They are also easily recognized because of their enormous Balmer jumps. A zero-point calibration for the luminosities of Population II yellow PAGB stars may be set with those in Galactic globular clusters (GCs).

The aim of this paper is to obtain the color-magnitude diagram (CMD) and distance of the little-studied southern GC, NGC 5986. This cluster is remarkable because it contains two candidate A-F type PAGB stars, discovered some years ago during a photographic grism survey (Bond 1977). Membership of the two PAGB stars in the cluster is confirmed by their radial velocities and by Strömgren photometry showing very low surface gravities (Bond 2001). This hitherto obscure cluster thus may be destined to fill a role comparable to that of the handful of galaxies that have produced more than one Type Ia supernova. Since the cluster contains two PAGB stars, questions of cluster distance and reddening drop out; hence their observed V magnitudes will provide direct evidence on the width of the Population II yellow PAGB LF.

The CMD of NGC 5986 was first studied by Harris, Racine, & DeRoux (1976) with photographic plates. A search for variable stars in the cluster was made by Liller & Lichten (1978), also with photographic plates. We present new CCD BV photometry of NGC 5986, including new light curves of the cluster’s RR Lyrae variables. Comparisons of our modern CCD photometry are made with the older studies. We provide new estimates of the cluster’s reddening and distance, and we derive the luminosities of the two candidate PAGB stars.

In addition to our study of the PAGB stars, it is also interesting to compare the CMD and the RR Lyrae stars of NGC 5986 to those of other Galactic GCs. Such comparisons remain an active area of research because they are relevant to the interrelated problems of the Oosterhoff dichotomy (Oosterhoff 1939) and the “second-parameter” effect (Sandage & Wildey 1967), with implications for the formation of the Galaxy (e.g., Lee, Demarque, & Zinn 1990, 1994). For example, a new, third Oosterhoff class may be emerging (Pritzl et al. 2000), which is not easily understood in the context of canonical stellar evolution theory. Also, new exceptions to a universal luminosity-metallicity relation for RR Lyrae stars have been found in both metal-rich (Layden et al. 1999; Pritzl et al. 2000) and metal-poor (Lee & Carney 1999; Clement & Shelton 1999) clusters. We discuss NGC 5986 in the context of these recent developments.

2. Observations and Data Reduction

Observations of NGC 5986 and standard star calibration fields were obtained by H.E.B. at the Cerro Tololo Inter-American Observatory (CTIO) with the 0.9 m telescope. All observations were made with broad-band B and V filters available at CTIO, which typically changed from run to run. Images of the cluster were obtained at an airmass close to unity. All frames were bias-corrected and flat-fielded in the standard manner. The different runs and detectors are summarized as follows.

In 1988, observations were made with the 300×500 pixel RCA5 chip that had a scale of $0''.494$ pixel $^{-1}$ and a field of view of $2'.5$ by $4'.1$. The cluster was observed in B and V at least once on each of 9 consecutive nights from February 22 to March 2 (twice on 2 nights). Typical exposures in B and V were 90 and 45 s, respectively. These observations are best-suited for our variability study. Unfortunately, the RCA's small field of view limits our search for variable stars to the central region of the cluster.

Subsequent observations were made on the night of 1990 June 16 with the Tek4 chip trimmed to 500×500 pixels. The plate scale of $0''.454$ pixel $^{-1}$ yielded a field of view $3'.7$ on a side. These observations included photometric calibration data and our longest exposures of the cluster: two frames of 1200 s each in B and two frames of 300 s each in V .

The most recent observations were made on the nights of 1997 June 1 and 1998 August 26 with the 2048×2048 pixel Tek 2K (“No. 3”) CCD chip that had a sampling of $0''.396$ pixel $^{-1}$ and a field of view $13'.5$ on a side. These frames covered a much larger sky area and thus yield the best statistics on the cluster giant branch and horizontal branch in the CMD. Exposures were 30 and 20 s in 1997 and 75 and 45 s in 1998, in the B and V filters, respectively. Photometric calibration data were obtained on both nights.

2.1. Photometric Calibration

As noted above, calibration frames were obtained in 1990, 1997, and 1998. These consisted of observations of Landolt (1992) standard-star fields repeated at different airmasses during each night. Photometry of the standard stars was obtained with DAOPHOT (Stetson 1987) with a large aperture radius ($\sim 8''.0$). Growth curves indicate that the aperture magnitudes closely measure the total observable flux. For each night, we photometered ~ 20 standard stars with known colors ranging over $(B - V) \sim -0.2$ to 1.5 and visual magnitudes of $V \sim 10$ to 12 (1990) or $V \sim 12$ to 16 (1997 & 1998).

Our aperture magnitudes and the known standard system magnitudes of Landolt (1992) were then used to derive coefficients of the transformation equations of the form:

$$B = b + c_0 + c_1(B - V) + c_2(X - 1.0), \quad (1)$$

$$V = v + d_0 + d_1(B - V) + d_2(X - 1.0), \quad (2)$$

where b and v are the aperture magnitudes, B and V are standard magnitudes, and X is airmass. The 1997 data showed significant scatter which we attribute to nonphotometric conditions; they are not considered further except for differential variable star photometry. The 1990 and 1998 data yielded best-fit coefficients of $(c_0, c_1, c_2) = (-4.546, +0.150, -0.190)$ and $(-2.997, -0.112, -0.250)$, and $(d_0, d_1, d_2) = (-3.921, -0.032, -0.140)$ and $(-2.678, -0.004, -0.120)$, respectively. The residual standard deviation of each fit is typically 0.025 mag. The solution residuals show no apparent trends with standard magnitude, color, or airmass.

2.2. Cluster Photometry

We employed DAOPHOT/ALLSTAR (Stetson 1987) to identify stars and derive profile-fitted photometry from the 1990 and 1998 frames of NGC 5986. Star lists were assembled in the usual manner, i.e. by iteratively searching star-subtracted images for more stars and concatenating these lists. Model point-spread functions (PSFs) were constructed with 7 and 25 isolated stars on each of the 1990 and 1998 frames, respectively. Mean aperture corrections for each frame were derived with these same sets of stars. The aperture corrections are uncertain at the $\sim 2\%$ and 1% levels in the 1990 and 1998 data, respectively. This difference can be attributed to crowding. After applying aperture corrections, each pair of b and v instrumental magnitudes was calibrated according to Eqs. 1 & 2. We employ instrumental colors, then iterate until the solutions converge.

As a check of our calibration, stars were identified in both the 1990 and 1998 B and V frames. Comparisons of the 50 brightest matched stars show that systematic zero-point offsets in each color are less than 2%, consistent with the calibration uncertainties estimated above. It is noted that the faintest stars identified in the 1990 frames have $V \sim 18.5$, while the 1998 frames yield a detection limit of $V \sim 20$. This suggests that $V \sim 18.5$ is the confusion limit in the crowded cluster center, which we confirm to be the case in the 1998 data as well. Since the photometry of faint stars near the cluster center is confusion limited, the 1990 frames do not yield a significant improvement in photometric accuracy relative to the 1998 frames despite the longer exposures.

For the remainder of this work, the BV photometry of NGC 5986 from the 1998 run serves as our fiducial calibration. Over 6000 stars were detected in both the B and V frames. These 1998 calibrated photometry data are summarized in Table 1 (the complete table is available only in the electronic edition of *The Astronomical Journal*). Note that the center of the cluster is located at $X=1025$, $Y=1025$ in the pixel coordinates provided, which can be used to define different radial distance cuts for CMD construction. The image is available from the authors upon request. Additional photometry of the cluster obtained for the variable star search is described in §2.3.

In Figure 1, we compare our calibrated photometry to that of the Harris et al. (1976) photographic study for ~ 25 stars in common. The Harris et al. (1976) photometry was calibrated with the photoelectric standard-star sequence of White (1971). Two of the White (1971) standard

stars are also compared in Figure 1. Despite the considerable scatter of the Harris et al. (1976) data, we find that our zero points agree to within ~ 0.05 mag, which we consider acceptable. The difference may suggest a modest degree of flux contamination from faint neighboring stars in the photoelectric standard-star sequence of White (1971).

The photographic B photometry of cluster variable stars by Liller & Lichten (1978) was calibrated relative to the Harris et al. (1976) data. In addition, their magnitudes were estimated “by eye” in several instances. Thus we consider their photometry to be of limited use as a check of our calibration. Kravstov et al. (1997) also presented photographic photometry of NGC 5986 which was calibrated with the photoelectric standard star sequence of Alcaino (1984). Unfortunately, none of the Alcaino (1984) standard stars lie within our field of view. Finally, Rosenberg et al. (2000) recently presented a VI color-magnitude diagram for NGC 5986 derived from CCD data as part of a large catalog of globular cluster CMDs. A visual comparison of their CMD with ours (see §3) suggests that no large zero-point discrepancy exists. Judging by the cluster giant branch and the blue horizontal branch, our CMD shows significantly less scatter than that obtained by Rosenberg et al. (2000; see their Fig. 20), although their CMD reaches a fainter limit. Rosenberg et al. suggest that NGC 5986 is affected by differential reddening. However, we do not see strong evidence for this in our CMD, which is constructed from stars only near the cluster center.

Further discussion of the CMD of NGC 5986 is deferred to §3, after the variable star content of the cluster is characterized.

2.3. Search for Variable Stars

As mentioned above, Liller & Lichten (1978) searched for variable stars in NGC 5986 with photographic plates. They identified 9 periodic variables; all are RR Lyrae variables. Of these, 2 are overtone pulsators (RRc; but one is actually a foreground star) and 7 are fundamental mode pulsators (RRab). The cluster also contains one bright, red semiregular variable and one severely blended variable star whose period was not determined.

The field of view of our 1988 RCA data includes the semiregular (V4), and the blended variable (V10). It also includes 5 of the RRab (V1, V2, V6, V9, and V11), and one RRc (V12); the latter is believed to be a foreground star and not a member of NGC 5986. The known variables lying outside of our field of view are V3, V8 (both are RRab), and V7 (an RRc). Note that V5 is actually a nonvariable star (Liller & Lichten 1978).

Given our modern CCD data, it seemed worth searching for new, possibly overlooked, variable stars in NGC 5986. In addition, we decided to experiment with a newly developed “difference imaging” analysis package. Difference imaging is well suited to the task of finding variable stars in crowded fields. In this type of analysis, all nonvariable stars are subtracted away in each frame, leaving isolated (and thus easy to photometer) images of only those stars which have changed

brightness relative to a fiducial frame (e.g., Alard 2000).

Our difference imaging analysis is briefly summarized as follows. First, closely spaced observations on the same nights were averaged to increase signal to noise. This yielded 10 V frames and 9 B frames over the 9 nights in 1988. Source lists for each frame were generated with SExtractor (Bertin & Arnouts 1996), frame-to-frame coordinate transformations were derived with the method of similar triangles (Groth 1986), and then all frames were transformed to a common coordinate system³. Next, B and V reference images were created by taking the medians of the transformed frames. Each frame was then subtracted from the appropriate reference image with the ISIS program (Alard 2000). We employed DAOPHOT to search the subtracted frames for 3σ , positive or negative, star-like images. In this manner, all of the known variables were recovered as 3σ detections in both B and V , and in at least 3 of the 9 pairs of BV frames over the 9 nights. No other stars met these criteria. A few dozen other candidate variables (i.e., 3σ detections in 1 or 2 pairs of BV frames) were carefully inspected, but each could be attributed to photon noise (i.e., subtractions of very bright stars) or defects in the image data. We estimate our detection limit for variability to be ~ 0.01 mag over a ~ 10 day period. Thus, based on this difference imaging analysis, we conclude that the variable star survey of NGC 5986 by Liller & Lichten (1978) was complete in the cluster center.

We then re-reduced the RCA frames with DAOPHOT/ALLSTAR in order to obtain PSF-fitted photometry in a manner consistent with the 1990, 1997, and 1998 reductions (see §2.2). For each photometry list, stars in common with the calibrated 1998 BV data were used to derive transformations from the instrumental ALLSTAR-reported magnitudes directly to calibrated B or V . These equations included only a zero-point and color term. The color coefficients so obtained were consistent with those found with the standard-star calibration data (see §2.1). We estimate that each photometric measurement is transformed to the Johnson BV system with an uncertainty of about 0.01 mag. In total, we made up to 12 two-color photometric measurements of each variable, spanning a 10 year period. These photometric data are summarized in Table 2.

The B and V light curves of the 5 cluster-member RR Lyrae stars are shown in Figure 2, including the Liller & Lichten (1978) photographic B data. No zero-point offsets have been applied to the photographic data. Since our new data extend the time baseline of observations by an additional ~ 15 years, we rederived the pulsation periods from the combined CCD and photographic B -band light curves with the supersmooth period-finding code (Reimann 1994). By inspection of the period-folded light curves (see Figure 3), we estimate minimum and maximum light (uncertainty of ± 0.05 mag), which also yields the pulsation amplitudes (A_V and A_B) and the $(B - V)$ colors at minimum light. The mean brightnesses are the intensity-weighted averages of the calibrated CCD data (see Table 2). These various characteristics of the light curves are summarized in Table 3. The average magnitudes of the RRab variables in NGC 5986 are $V(\text{RR}) = 16.52 \pm 0.04$ and $B(\text{RR}) = 17.28 \pm 0.04$.

³The image “remapping” was accomplished with code written by J. Tonry.

3. The NGC 5986 Color-Magnitude Diagram

In Figure 3 we show the CMD for all stars lying within $3'$ of the center of NGC 5986. The time-averaged magnitudes and colors of the cluster's variables (5 RRab and 1 SR) are distinguished, as are the 2 (nonvariable) PAGB stars. Some contamination from field stars is clearly present in spite of the small radius cut chosen for the CMD. However, major features such as the red giant branch (RGB), blue horizontal branch (HB), and the red-giant-branch bump (RGB-bump) near $V \approx 16.5$, are easily identified. Our photometry does not reach the cluster's subgiant branch or main sequence turn-off. The small number of stars associated with the cluster's asymptotic-giant-branch bump (AGB-bump) are a bit confused with field star interlopers, but this feature is located at $V \approx 15.5$, and $(B - V) \approx 1.0$. The RRab stars define the location of the cool, red portion of the cluster's HB, which is otherwise difficult to distinguish. The semiregular variable, V4, is a bit brighter than the tip of the RGB, and is thus probably located very near the end (or tip) of the AGB. The nonvariable PAGB stars (Bond 2001) are bluer than the RR Lyrae variables. Thus the blue edge of the Population II instability strip is seen to lie at $(B - V) \approx 0.6$ (reddened value) in NGC 5986. Finally, we note that the single yellow star which is brighter than the 2 PAGB stars in Figure 3 is not a cluster member (Bond 2001).

The NGC 5986 HB is predominantly blue. We count the blue and red HB stars by defining appropriate regions of the CMD. The latter are assumed to be redder than the RRab but bluer than the RGB. In what follows, we use b , v , and r to denote the number of blue, variable, and red HB stars, respectively. We estimate $b \approx 300$ and $r \approx 10$. The cluster has a total of 7 RR Lyrae stars, but only 5 lying within $3'$; thus we define $v = 5$. Construction of CMDs corresponding to an equal area of sky, but located as far away from the cluster center as our data allow, suggest that field star contamination of the red HB star counts (r) is of order a few stars, while such contamination of the blue HB star counts (b) is probably negligible. These star counts yield an HB morphology index (e.g., Lee, Demarque, & Zinn 1990) of $(b - r)/(b + v + r) \approx 0.92$.

The clustering of stars on the red giant branch at $V(\text{bump}) = 16.470 \pm 0.025$ mag is identified as the RGB-bump (e.g., Ferraro et al. 1999; Alves & Sarajedini 1999). The location of the RGB-bump is determined by fitting the cluster's differential giant branch luminosity function with a model function, as shown in Figure 4. The fitted model function is a Gaussian of arbitrary height, width, and center, and a 3-parameter (quadratic) background. The quadratic background accounts for the underlying RGB while the Gaussian represents the RGB-bump. A chi-squared minimization yields the best-fit center for the peak of the Gaussian and associated error, which we report above.

Guided by the cluster's RRab stars, we determine the color of the red giant branch at “the level of the HB” to be $(B - V)_g = 1.055 \pm 0.005$. This formal error does not account for our photometric calibration. Our measurement of $(B - V)_g$ is made by fitting a Gaussian of arbitrary height, width, and center to a color-frequency histogram of RGB stars in the range $V = 16.3$ to 16.9. We adopt the best-fit center and associated error as the nominal RGB color. Note that

different V magnitude cuts centered on the mean brightness of the RRab yield consistent results.

3.1. Metallicity

The metallicity of NGC 5986 is well-constrained by observations other than our own, such as the integrated light of the cluster (Zinn & West 1984), and spectroscopic measurements of the Ca II triplet for several of the cluster's red giants (Rutledge et al. 1997). Rutledge, Hesser & Stetson (1997b) estimate the metallicity as $[\text{Fe}/\text{H}]_{ZW84} = -1.65 \pm 0.04$ on the Zinn & West (1984) scale, or $[\text{Fe}/\text{H}]_{CG97} = -1.35 \pm 0.04$ on the Carretta & Gratton (1997) scale. The color of the NGC 5986 giant branch in the Washington system and an assumption for the cluster's reddening yields a consistent result (Geisler, Claria, & Minniti 1997). For the purposes of this work, we assume that the metallicity of NGC 5986 is a known parameter, as listed above on each of the two currently popular metallicity scales.

It is interesting to compare the known metallicity with that derived from the periods and amplitudes of the cluster's RRab variables. Using the calibration of Walker & Mack (1986) in terms of the B -band pulsation amplitude (A_B) and period, we find $[\text{Fe}/\text{H}]_{ZW84} = -2.26 \pm 0.06$. The calibration of Alcock et al. (1999) in terms of A_V and period yields $[\text{Fe}/\text{H}]_{ZW84} = -2.33 \pm 0.08$. These estimates are clearly at odds with the metallicity derived from the spectroscopy of giants and the integrated cluster light, which suggests a systematic difference between the RRab variables in NGC 5986 and the calibrating RRab stars. This will be discussed further in §4.

3.2. Reddening

We first consider two published results for the reddening toward NGC 5986. Zinn's (1980) analysis of the cluster's integrated colors yields $E(B - V) = 0.29 \pm 0.05$, while the reddening maps of Burstein & Heiles (1982) indicate $E(B - V) = 0.27 \pm 0.10$. The stated uncertainties in these two measurements were assigned by us after a careful review of the data.

We also calculate the reddening with our new BV photometry. First, the colors of the cluster's RRab variables at minimum light yield an estimate of the reddening; this is known as Sturch's (1966) method. Employing the calibration from Walker (1990), and the period and color data from Table 3, we estimate $E(B - V) = 0.36 \pm 0.05$. The uncertainty here is dominated by the error of the mean color at minimum light for the 5 RRab listed in Table 3. Next, using $(B - V)_g$ as derived above, $[\text{Fe}/\text{H}]_{CG97}$ from Rutledge et al. (1997b), and the calibration of Ferraro et al. (1999) for the intrinsic color of the giant branch, $(B - V)_{0,g}$, as a function of $[\text{Fe}/\text{H}]_{CG97}$ (their Eqn. 4.15), we find $E(B - V) = 0.26 \pm 0.04$. This uncertainty is dominated by the Ferraro et al. (1999) calibration.

For the remainder of this work, we adopt the weighted average of the four reddening estimates

summarized above: $E(B - V) = 0.29 \pm 0.02$.

3.3. Distance

In a cluster like NGC 5986, which has a predominantly blue HB and only a handful of RR Lyrae variables, it is difficult to determine the precise level of the zero-age horizontal branch (ZAHB; e.g., Ferraro et al. 1999). Since the RGB-bump is not subject to horizontal-branch evolutionary effects, we calculate the distance to NGC 5986 with this feature. Adopting a standard reddening law ($R_V = 3.1$; Cardelli, Clayton, & Mathis 1989), the dereddened brightness of the RGB-bump is $V_0(\text{bump}) = 15.570 \pm 0.065$. This uncertainty accounts for uncertainties in the reddening and our measurement of $V(\text{bump})$. The calibration of Ferraro et al. (1999) in terms of $[\text{Fe}/\text{H}]_{CG97}$ predicts $M_V(\text{bump}) = 0.425 \pm 0.08$, where the uncertainty represents the standard deviation of the calibration combined with the uncertainty in $[\text{Fe}/\text{H}]_{CG97}$ for NGC 5986 (see §3.1). Thus we arrive at true distance modulus of $(m - M)_0 = 15.15 \pm 0.10$, or a distance of 10.72 ± 0.50 kpc.

At this distance, the RRab variables in NGC 5986 have a mean absolute visual magnitude of $M_V(\text{RR}) = 0.47 \pm 0.11$. For comparison, the calibration⁴ of Chaboyer et al. (1998) predicts $M_V(\text{RR}) = 0.45$. Thus the distance to NGC 5986 derived from the RR Lyrae variables and this calibration would be in good agreement with our estimate based on the RGB-bump.

4. The RR Lyrae Variables in NGC 5986

The RRab stars in the Bailey diagram ($\log P$ vs. A_V ; see Table 3) are shown in Figure 5. We compare the RRab stars in NGC 5986, the one RRab star in M15 (Pike & Meston 1977), and the RRab stars in M3 from Kaluzny et al. (1998) and Carretta et al. (1998). Fiducial “ridge” lines for the RRab variables in M3 and M15 are taken from Alcock et al. (1999). These ridge lines illustrate the use of the Bailey diagram as a diagnostic of metallicity. RRab stars with lower metallicities have longer periods at a fixed amplitude (i.e., M15 is more metal-poor than M3). However, despite having nearly identical metallicities, the RRab stars in NGC 5986 and M13 are unlikely to be drawn from the same distribution as the RRab in M3 in this diagram. The former lie at noticeably longer periods. This systematic period shift explains the failure of the periods and pulsation amplitudes of the RRab stars in NGC 5986 to predict the metallicity of the cluster (see §3.1).

Lee & Carney (1999) have pointed out a similar problem with the RRab variables in M2 (also in a comparison with those in M3). Thus the RRab stars in 3 clusters (NGC 5986, M2, and

⁴Chaboyer et al. (1998) find $M_V(\text{RR}) = 0.23(\pm 0.03) \cdot ([\text{Fe}/\text{H}]_{ZW84} + 1.9) + 0.39(\pm 0.08)$.

M13) have systematically longer periods than those in the cluster M3, yet all of these clusters have nearly the same metallicity. It is interesting that the 3 clusters with the long-period RRab variables all have blue HBs, $(b - r)/(b + v + r) \approx 0.9$, while M3 has $(b - r)/(b + v + r) \approx 0.1$. Clement & Shelton (1999) have argued that the location of cluster RRab stars in the Bailey diagram is not a unique function of metallicity. They suggest that the period-shift effect seen here is due to the higher luminosities of the RRab stars, which are in a relatively more advanced evolutionary state.

We compare the luminosities of the RRab variables in NGC 5986 and M3 as follows. From Lee & Carney (1999), who reanalyzed the M3 cluster photometry of Ferraro et al. (1997) and the M3 RR Lyrae photometry of Carretta et al. (1998), the average brightness of the RRab stars is $V(\text{RR}) = 15.665 \pm 0.001$. Ferraro et al. (1997) identified the RGB-bump in M3, and found $V(\text{bump}) = 15.45 \pm 0.05$. The reddening toward M3 is low, $E(B - V) = 0.01$; thus the dereddened brightnesses are $V_0(\text{RR}) = 15.63$ and $V_0(\text{bump}) = 15.42$. Rutledge et al. (1997b) give $[\text{Fe}/\text{H}]_{\text{CG97}} = -1.34 \pm 0.04$ for M3. Therefore, the RGB-bump luminosity in M3 should be the same as in NGC 5986, or $M_V(\text{bump}) = 0.425$. The true M3 distance modulus is then $(m - M)_0 = 15.00 \pm 0.10$, and the mean absolute visual magnitude of the RRab stars is $M_V(\text{RR}) = 0.63 \pm 0.11$. This compares with $M_V(\text{RR}) = 0.47 \pm 0.11$ found for NGC 5986. Assuming that $M_V(\text{bump})$ is the same for both M3 and NGC 5986, the relative brightness difference between the two groups of RRab stars is $\Delta V(\text{RR}) = 0.17 \pm 0.07$, where ΔV is defined in the sense of M3 – NGC 5986.

As a check, the luminosity difference can also be inferred from the period shift in the Bailey diagram. We estimate that the RRab variables in NGC 5986 are shifted by $\Delta \log P \approx -0.07$ dex relative to the M3 ridge line shown in Figure 4. Following Lee & Carney (1999), if the average masses of the RR Lyrae stars in each cluster are the same, the pulsation equation implies a luminosity difference of $\Delta \log(L/L_\odot) \approx -0.08$ dex for this period shift. If the bolometric corrections are the same in each cluster, this luminosity difference corresponds to $\Delta V(\text{RR}) \approx 0.20$ mag, in good agreement with our estimate above. This agreement also supports the assumption that the masses of RRab stars in M3 and NGC 5986 are the same. In summary, the RRab stars in NGC 5986 appear to be about 0.2 mag brighter on average than those in M3.

Our comparison of the RRab stars in NGC 5986 and M3 demonstrates an unambiguous exception to a universal $M_V(\text{RR})$ – $[\text{Fe}/\text{H}]$ relation. A similar conclusion was reached by Lee & Carney (1999) and Clement & Shelton (1999) based on their analyses of the RR Lyrae stars in other metal-poor clusters. Exceptions to a universal $M_V(\text{RR})$ – $[\text{Fe}/\text{H}]$ relation have also been found for RR Lyrae stars in metal-rich GCs (Layden et al. 1999; Pritzl et al. 2000). It is not clear that the exceptions in the metal-poor and metal-rich clusters can be explained by the same physical process. For the case of the NGC 5986, we suggest that the RRab stars have evolved off of the blue ZAHB and into the instability strip at higher luminosities, while those in M3 are on average less evolved, closer to their ZAHB locations, and fainter.

5. The PAGB Stars in NGC 5986

The use of A-F spectral type (“yellow”) post-AGB stars as Population II standard candles has been championed by Bond and collaborators (e.g., Bond 1997, Bond & Fullton 1997, Bond 2001). As discussed in §1, the two candidate PAGB stars in NGC 5986 allow a test of the assertion that the V -band luminosity function (LF) of Population II yellow PAGB stars should be sharply peaked.

Our new BV photometry (Table 1) and analysis of the NGC 5986 distance yield $M_V = -3.40$ and -3.30 for the stars PAGB-1 and PAGB-2, respectively. Thus, based on only these two stars, we suggest that the LF of Population II yellow PAGB supergiants peaks near $M_V = -3.35 \pm 0.05$.

The bolometric corrections of Flower (1996) yield $\log L/L_\odot = 3.31$ and 3.21 for PAGB-1 and PAGB-2, respectively. The luminosity-core mass calibration of Vassiliadis & Wood (1994), which is independent of metallicity over the range of models calculated, then predicts masses of $M = 0.536$ and $0.528 M_\odot$, respectively. Thus the typical PAGB remnant mass in NGC 5986 is about $0.53 M_\odot$. This is in fair agreement with the average mass of white dwarfs in GCs and the halo field, $M = 0.50 \pm 0.02 M_\odot$, as recently reviewed by Alves, Bond, & Livio (2000, and references therein).

For comparison, we estimate that the semiregular variable V4 in NGC 5986 has $\log L/L_\odot = 3.44$, which is higher than both PAGB stars. In this case, Whitelock’s (1986) period-luminosity calibration implies a period of about 300 days, which would be one of the longest periods known for semiregulars in GCs. Our data suggest a period of order $\gtrsim 20$ days. However, a period as long as 300 days seems unlikely. If this star leaves the AGB and evolves at constant luminosity to higher temperatures, it would appear as a yellow PAGB star with $M_V \sim -3.85$. We caution that the BV bolometric correction (Flower 1996) we have employed for this cool, metal-poor giant is large and uncertain. In this regard, near-infrared photometry would be useful. Radial velocity data are also needed to confirm this star’s cluster membership.

Based on only the two yellow PAGB stars in NGC 5986, the intrinsic scatter, or width, of the peak of V -band LF appears to be quite narrow. However, we are obviously dealing with small-number statistics. There is one other well-known yellow PAGB star in a GC; this is ROA 24 in ω Cen, a confirmed cluster member. Adopting the BV photometry assembled by González & Wallerstein (1992), and the reddening and distance modulus from Alcaino & Liller (1987; see also Harris 1996), we estimate⁵ $M_V = -3.15 \pm 0.12$, $\log L/L_\odot = 3.17$, and $M = 0.526 M_\odot$. ROA 24 combined with the two PAGB stars in NGC 5986 suggests that the intrinsic width of the V -band yellow PAGB LF is $\sigma_V \sim 0.10\text{--}0.15$ mag, with a peak at $M_V(PAGB) = -3.28 \pm 0.07$.

Recently, Neely, Sarajedini, & Martins (2000) presented a new CMD of the GC NGC 6144,

⁵We note that M_V for ROA 24 in González & Wallerstein (1992) was incorrectly calculated from V and $(m - M)_0$ instead of $(m - M)_V$.

and suggested that this cluster also contains a yellow PAGB star. Using the M_V (RR) calibration of Chaboyer (1998) as in §3.3, and the reddening, metallicity, and V (HB) estimates from Neely et al. (2000), this candidate yellow PAGB star has $M_V = -4.04$, $\log L/L_\odot = 3.51$, and $M = 0.56M_\odot$. Based on this high luminosity and mass, we suggest that this star may not be a member of the cluster. Measurement of the Balmer jump would confirm the PAGB nature of this star. Radial velocity data are also needed to confirm its cluster membership.

The existence of *two* yellow PAGB stars in NGC 5986 argues that their lifetimes are relatively long. Extant stellar evolution theory cannot predict yellow PAGB lifetimes in an absolute sense, because the transition from the tip of the AGB to yellow PAGB star is critically dependent on ad hoc mass-loss parameterizations (Trams et al. 1989; Vassiliadis & Wood 1994). This is not the case for hotter PAGB stars, such as the nuclei of PNe, whose evolutionary timescales are less sensitive to the mass-loss rates. If yellow PAGB stars live $2\text{--}3 \times 10^4$ years, and assuming each star in a GC becomes a yellow PAGB star, the total luminosity of the GC system implies a total of ~ 16 yellow PAGBs in GCs. Based on the 3 known PAGB stars in the GC system (2 in NGC 5986 and 1 in ω Cen), a minimum lifetime is $\gtrsim 4000$ years. However, we remind that no systematic search of the GC system for yellow PAGBs has yet been conducted.

The calibration of yellow PAGB stars as standard candles will require a larger sample of objects, probably of order a dozen stars in Galactic GCs, in order to accurately define the peak and width of the V -band LF. Close-binary merger scenarios may introduce outliers on the bright side of what may otherwise be a sharply peaked LF (e.g., Alves et al. 2000). Nonvariable stars lying blueward of the Population II instability strip, but in an evolutionary state related to the Population II Cepheids, may introduce outliers on both the faint and bright sides of the LF. Indeed, some Population II Cepheids in GCs reach luminosities of $M_V \sim -3.5$ (e.g., González & Wallerstein 1992). If yellow “cousins” of the Population II Cepheids significantly contaminate the PAGB LF, we predict a correlation between the occurrence of yellow PAGBs in GCs and the clusters’ HB morphologies, as the Population II Cepheids show (Wallerstein 1970). We have undertaken a large-scale survey of the GC system for yellow PAGB stars, which will help to define observationally the true peak and width of their V -band LF, and perhaps shed new light on the unusual presence of *two* PAGB stars in NGC 5986.

6. Conclusion

We have presented a new BV color-magnitude diagram of NGC 5986, as well as new BV light curves for 5 of the cluster’s RR Lyrae variables. We have detected the RGB-bump for the first time on this cluster’s giant branch. Our analysis of the color-magnitude diagram yields new estimates for the reddening and true distance modulus: $E(B - V) = 0.29 \pm 0.02$ and $(m - M)_0 = 15.15 \pm 0.10$, respectively. In comparison with the globular cluster M3, which has the same metallicity as NGC 5986, we find that the RR Lyrae stars in the latter are about 0.2 mag brighter. This is an important exception to a universal M_V (RR)–[Fe/H] relation in a metal-poor

cluster. Our BV photometry of the two candidate yellow PAGB stars in NGC 5986 suggests that the V -band LF of these stars is sharply peaked at $M_V(\text{PAGB}) = -3.28 \pm 0.07$.

This work was partially supported by NASA grant NAG5-6821 under the “UV, Visible, and Gravitational Astrophysics Research and Analysis” program. H.E.B. thanks the staff at Cerro Tololo for their support over the years.

REFERENCES

Alcock, C. et al. 1999, AJ, 119, 2194
Alves, D.R., & Sarajedini, A. 1999, ApJ, 511, 225
Alves, D.R., Bond, H.E., & Livio, M. 2000, AJ in press: astro-ph/0007190
Alard, C. 2000, A&AS, 114, 363
Alcaino, G. 1984, A&A, 139, 549
Alcaino, G., & Liller, W. 1987, A&A, 94, 1585
Bertin, E., & Arnouts, S. 1996, A&AS, 117, 393
Bond, H.E. 1977, BAAS, 9, 601
Bond, H.E. 1997, in The Extragalactic Distance Scale, eds. M. Livio, M. Donahue, & N. Panagia (Cambridge: Cambridge University Press), 224
Bond, H.E., & Fullton, L. K. 1997, BAAS, 29, 843
Bond, H.E. 2001, in preparation
Burstein, D., & Heiles, C. 1982, AJ, 87, 1165
Cardelli, J.A., Clayton, G.C., & Mathis, J.S. 1989, ApJ, 345, 245
Carretta, E., & Gratton, R.G. 1997, A&AS, 121, 95
Carretta, E. et al. 1998, MNRAS, 298, 1005
Chaboyer, B., Demarque, P., Kernan, P.J., & Krauss, L.M. 1998, ApJ, 494, 96
Clement, C.M., & Shelton, I. 1999, ApJ, 515, L85
Ferraro, F.R. et al. 1997, A&A, 320, 757
Ferraro, F.R. et al. 1999, AJ, 118, 1738
Flower, P.J. 1996, ApJ, 469, 355
Geisler, D., Claria, J.J., & Minniti, D. 1997, PASP, 109, 799
González, G., & Wallerstein, G. 1992, MNRAS, 254, 343
Groth, E. 1986, AJ, 91, 1244
Harris, W.E., 1996, AJ, 112, 1487
Harris, W.E., Racine, R., & De Roux, J. 1976, ApJS, 31, 13
Kaluzny, J., Hilditch, R., Clement, C., & Rucinski, S. 1998, MNRAS, 296, 347
Kravstov, V.V. et al. 1992, Astronomy Letters, 23, 391
Landolt, A.U. 1992, AJ, 104, 340
Layden, A.C., Ritter, L.A., Welch, D.W., & Webb, T.M.A., 1999, AJ, 117, 1313
Lee, J.-W., & Carney, B.W. 1999, AJ, 118, 1373

Lee, Y.-W., Demarque, P., & Zinn, R. 1990, *ApJ*, 350, 155
Lee, Y.-W., Demarque, P., & Zinn, R. 1994, *ApJ*, 423, 248
Liller, M.H., & Lichten, S.M. 1978, *AJ*, 83, 1070
Neely, R.K., Sarajedini, A., & Martins, D.H. 2000, *AJ*, 119, 1793
Oosterhoff, P.Th. 1939, *Observatory*, 62, 104
Pike, C.D., & Meston, C.J. 1977, *MNRAS*, 180, 613
Pritzl, B., Smith, H.A., Catelan, M., & Sweigart, A.V. 2000, *ApJ*, 530, L41
Reimann, J., 1994, Ph.D. dissertation, U.C. Berkeley
Rutledge, G.A. et al. 1997, *PASP*, 109, 883
Rutledge, G.A., Hesser, J.E., & Stetson, P.B. 1997, *PASP*, 109, 907
Rosenberg, A., Piotto, G., Savianne, I., & Aparicio, A., 2000, *A&AS*, in press: astroph/0002205
Sandage, A., & Wildey, R. 1967, *ApJ*, 150, 469
Stetson, P. 1987, *PASP*, 99, 191
Sturch, C. 1966, *ApJ*, 143, 774
Trams, N.R. et al. 1989, *A&A*, 218, L1
Walker, A. 1990, *AJ*, 100, 1532
Walker, A., & Mack, P. 1986, *MNRAS*, 220, 69
Wallerstein, G. 1970, *ApJ*, 160, 345
White, R.E. 1971, *AJ*, 76, 419
Whitelock, P. 1986, *MNRAS*, 219, 525
Vassiliadis, E., & Wood, P. 1994 *ApJS*, 92, 125
Zinn, R. 1980, *ApJS*, 42, 19
Zinn, R., & West, M.J. 1984, *ApJS*, 55, 45

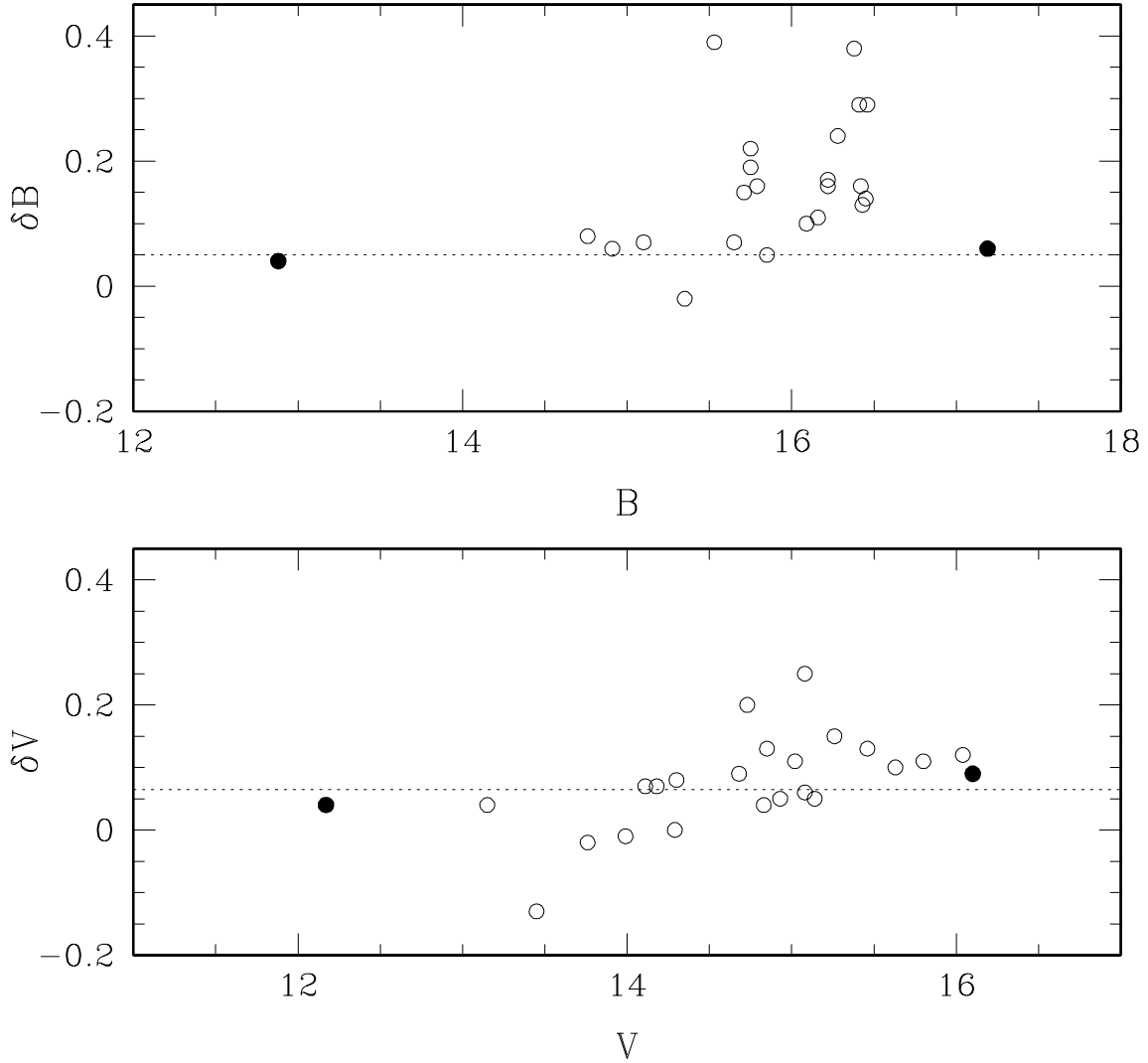


Fig. 1.— Comparison of our calibrated photometry with the photographic photometry of Harris et al. (1976; shown as open circles) and the photoelectric standard sequence photometry of White (1971; shown as filled circles). In each panel, we plot the magnitude difference (δB and δV = this work – past work) as a function of our calibrated magnitudes (B and V). The dotted lines show the mean offsets calculated from the two photoelectric standard stars.

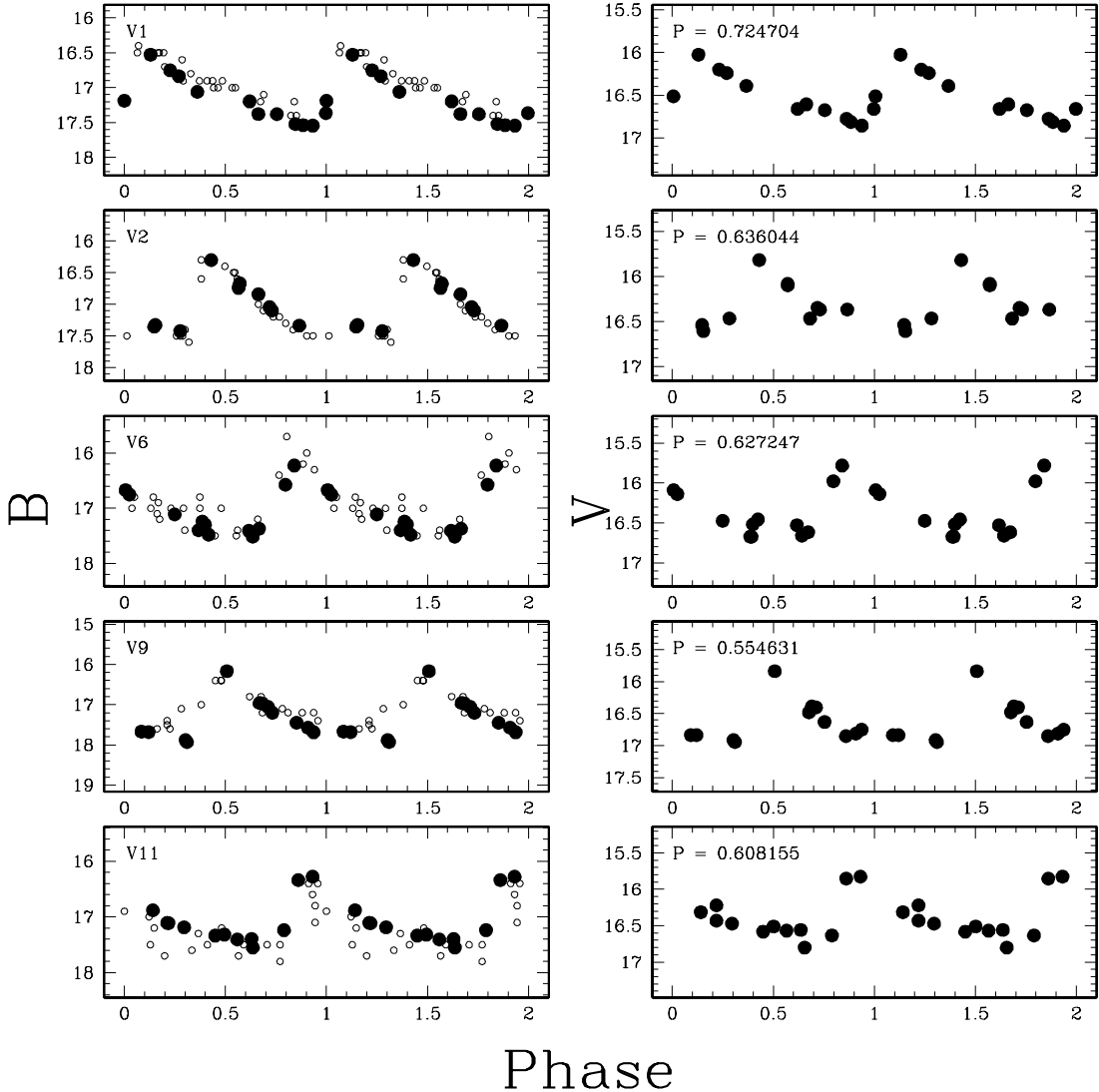


Fig. 2.— Period-folded light curves of 5 type ab RR Lyrae in NGC 5986. The B and V light curves are shown in the left and right panels, respectively. The variable identifier is labeled in the B panel. The period is labeled in the V panel. Our new photometric data are indicated with filled circles. The photographic B photometric data from Liller & Lichten (1978) are shown with open circles. The periods have been refined using the combined datasets, but are in good agreement with the original estimates by Liller & Lichten (1978).

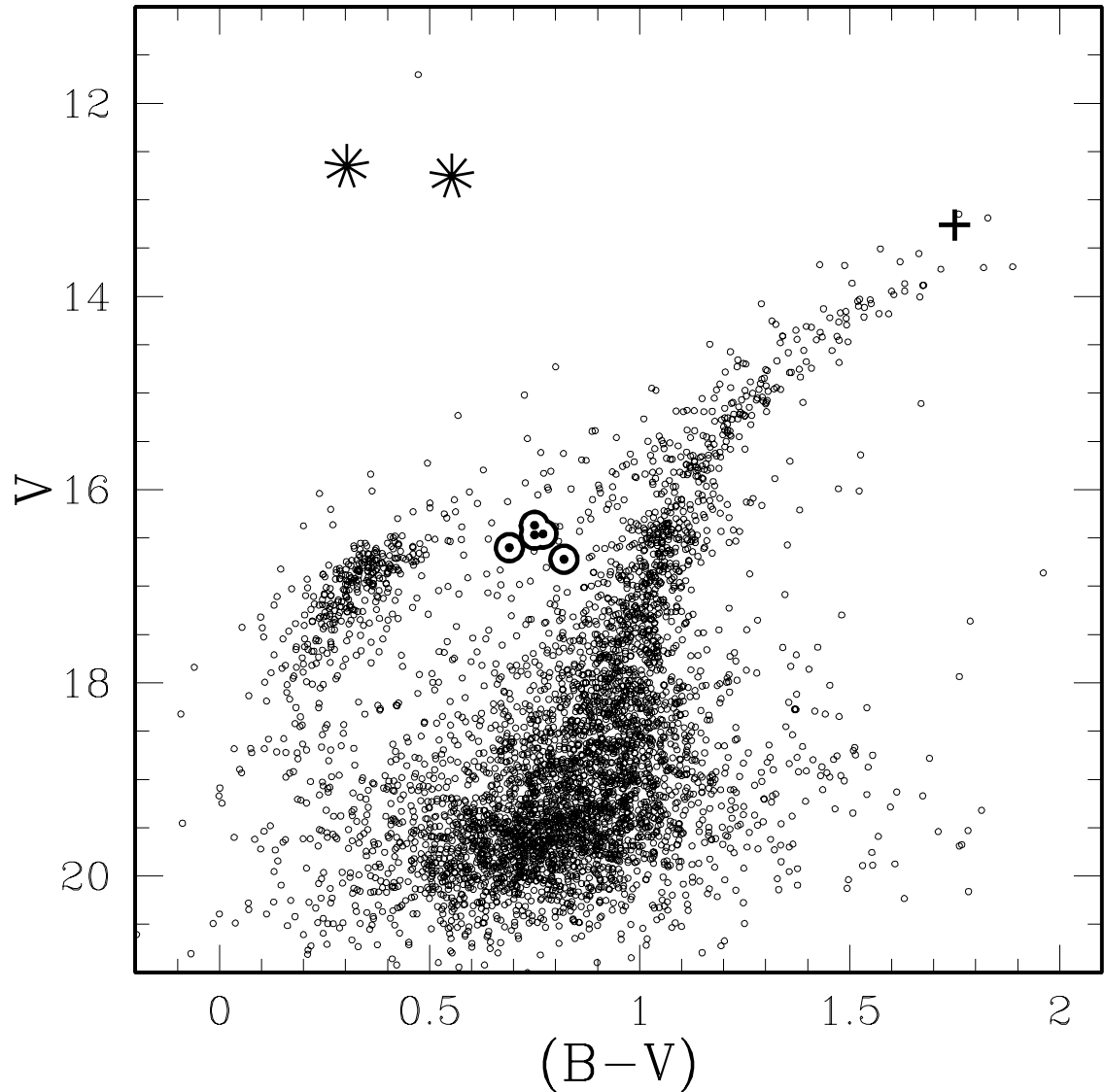


Fig. 3.— CMD of NGC 5986; all stars within $3'$ of the cluster center are plotted. Five RRab stars are shown with bulls-eyes (intensity-weighted average positions). The cluster's semiregular variable is marked with a plus. The two PAGB stars are shown with asterisks; note also the one foreground star of similar brightness and color (Bond 2000).

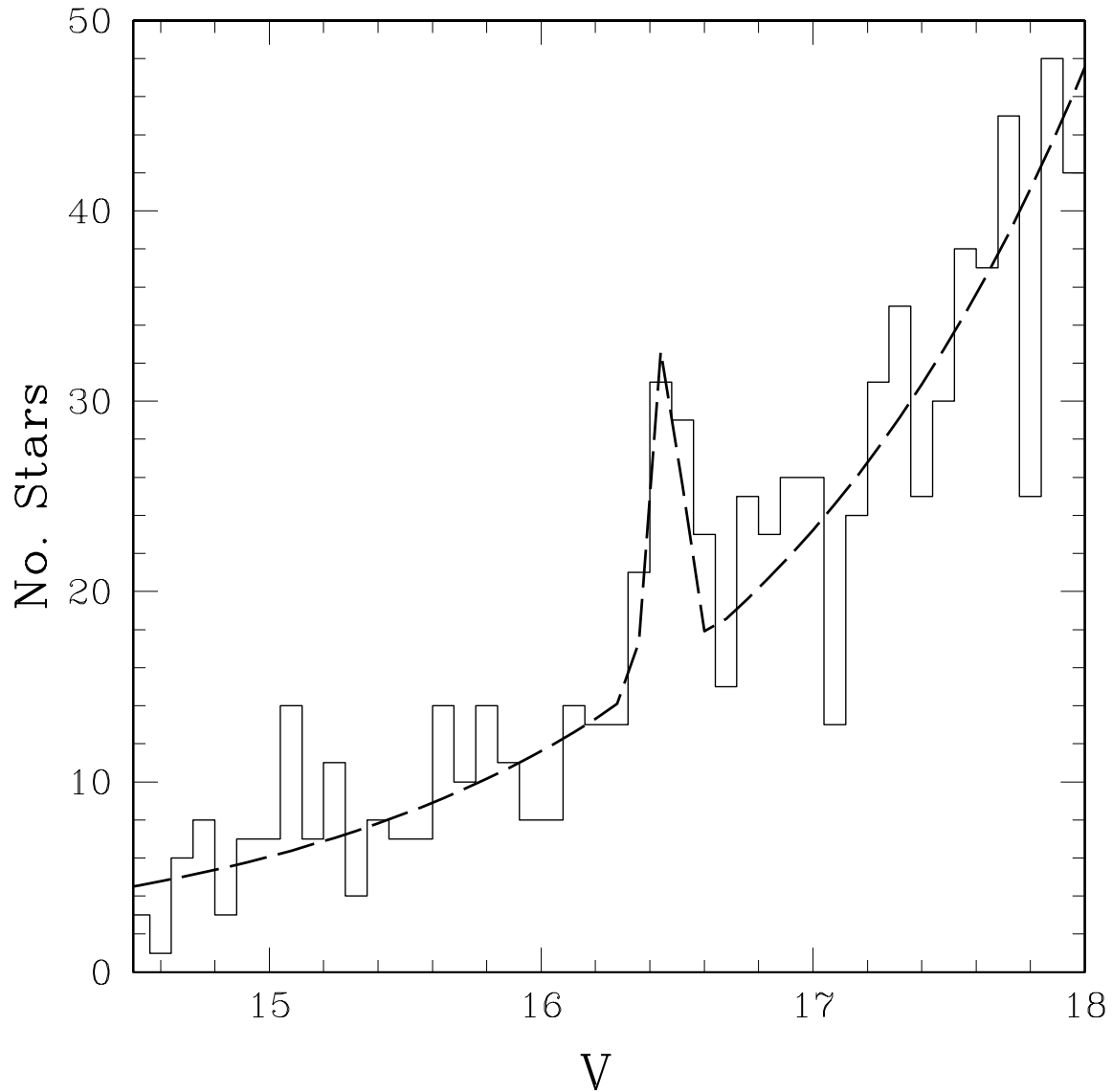


Fig. 4.— The cluster's giant branch differential luminosity function (histogram), with our best fit model function overplotted (dashed line). The RGB-bump is peaks at $V = 16.47 \pm 0.03$.

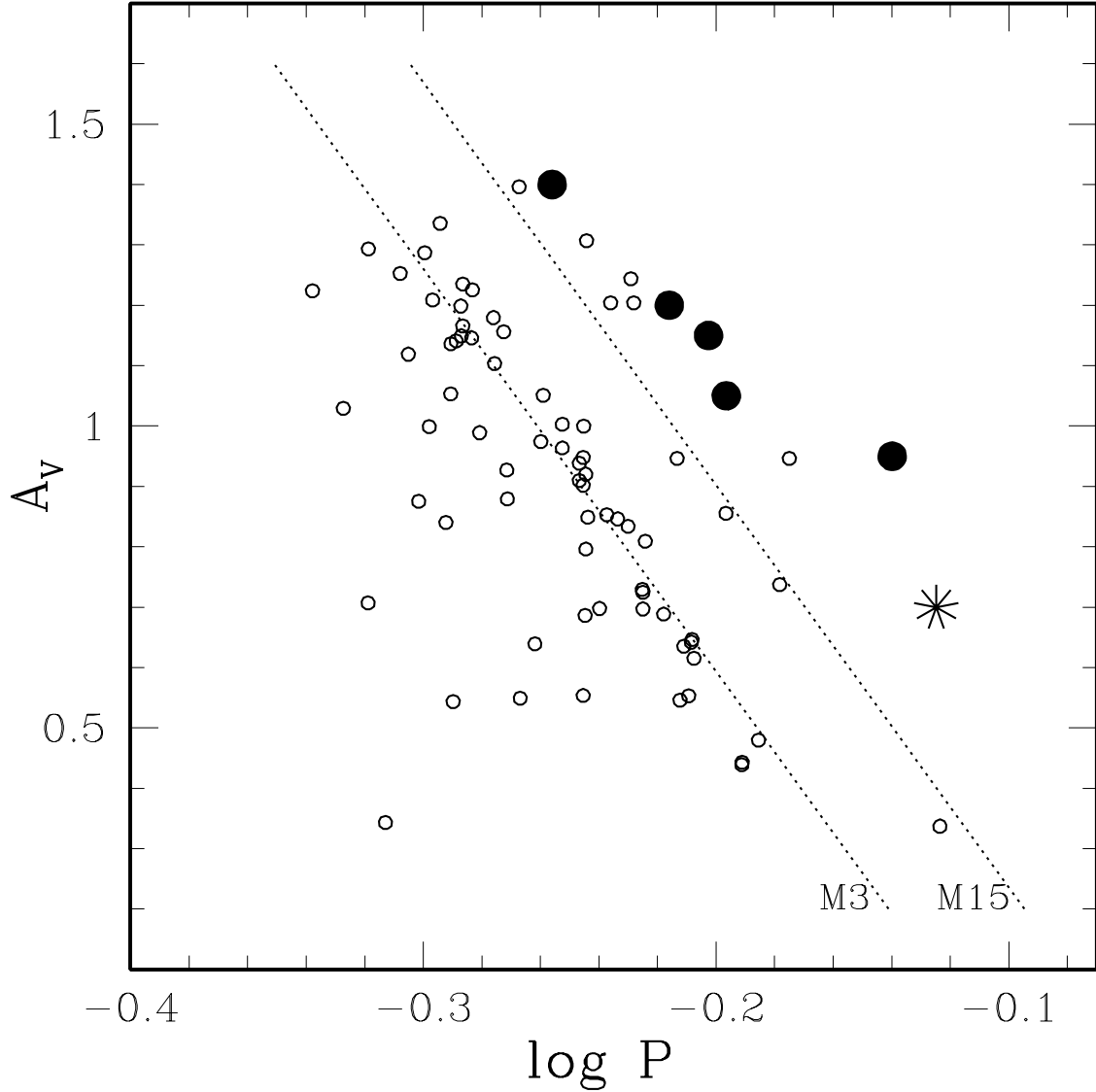


Fig. 5.— The Bailey period-amplitude diagram. The RRab in NGC 5986 are plotted as bold filled circles. We plot the RRab in M3 from Kaluzny et al. (1998) and Carretta et al. (1998) as small open circles. The one RRab in the cluster M13 is shown with an asterisk (Pike & Meston 1977). Fiducial “ridge” lines for the RRab in the clusters M3 and M15 are indicated with dotted lines and labeled.

Table 1. Calibrated *BV* Photometry of NGC 5986 and Surrounding Field

ID	X _{PIX} ^a	Y _{PIX} ^a	<i>B</i>	σ_B	<i>V</i>	σ_V	Comment ^b
1	874.035	977.380	12.176	0.008	11.703	0.014	Star F
2	317.649	1486.862	12.876	0.019	12.169	0.015	
3	1636.164	1269.349	13.957	0.018	12.503	0.013	
4	242.104	1859.430	13.833	0.028	12.560	0.024	
5	1605.885	836.089	13.502	0.012	12.617	0.011	
6	1013.955	964.771	12.955	0.010	12.652	0.010	PAGB-1
7	966.942	1010.151	13.308	0.008	12.755	0.014	PAGB-2
8	1801.448	1977.540	13.682	0.035	12.879	0.031	

NOTE – Table 1 is presented in its entirety in the electronic edition of the Astronomical Journal. A portion is shown here for guidance regarding its form and content.

^aPixel coordinates from 1998 data; the plate scale is $0''.396 \text{ pixel}^{-1}$ The center of the cluster is at approximately X = 1025, Y = 1025.

^bStar F is a foreground F dwarf. PAGB-1 and PAGB-2 are the two PAGB candidates, denoted “BW” and “BE” in Bond (2000). Known variable star designations (i.e., V4) are also listed in the complete version of this table.

Table 2. Time-Series BV Photometry of Variable Stars

ID	V	σ_V	H.J.D. $_V$	B	σ_B	H.J.D. $_B$
			2,400,000+			2,400,000+
V1	16.200	0.010	47213.902	16.752	0.013	47213.898
	16.662	0.026	47214.910	17.197	0.039	47214.910
	16.662	0.022	47215.906	17.365	0.021	47215.906
	16.392	0.009	47216.898	17.060	0.022	47216.895
	16.676	0.017	47217.906	17.380	0.029	47217.906
	16.025	0.010	47218.902	16.526	0.012	47218.902
	16.816	0.020	47220.898	17.538	0.025	47220.898
	16.240	0.009	47221.902	16.836	0.011	47221.902
	16.608	0.013	47222.910	17.377	0.024	47222.910
	16.777	0.014	48058.641	17.521	0.015	48058.629
	16.857	0.030	50601.676	17.544	0.030	50601.672
	16.513	0.013	51052.496	17.187	0.016	51052.492
V2	16.084	0.019	47213.902	16.743	0.024	47213.898
	16.606	0.039	47214.910	17.327	0.041	47214.910
	16.348	0.031	47215.906	17.045	0.027	47215.906
	16.465	0.020	47216.898	17.424	0.056	47216.895
	16.367	0.033	47217.906	17.337	0.034	47217.906
	15.819	0.020	47218.902	16.303	0.019	47218.902
	16.099	0.032	47220.898	16.672	0.026	47220.898
	16.538	0.030	47221.902	17.354	0.037	47221.902
	16.368	0.027	47222.910	17.099	0.027	47222.910
	16.467	0.066	48058.641	16.843	0.027	48058.629
	16.334	0.019	51052.496	16.929	0.014	51052.492
V4	13.373	0.004	47213.902	15.122	0.003	47213.898
	13.310	0.006	47214.910	15.067	0.010	47214.910
	13.292	0.005	47215.906	15.049	0.007	47215.906
	13.278	0.006	47216.898	15.016	0.008	47216.895
	13.208	0.005	47217.906	14.984	0.006	47217.906
	13.207	0.005	47218.902	14.940	0.005	47218.902
	13.168	0.009	47220.898	14.869	0.011	47220.898
	13.154	0.007	47221.902	14.866	0.006	47221.902
	13.149	0.004	47222.910	14.840	0.004	47222.910
	13.368	0.015	48058.641	15.128	0.004	48058.629
	13.219	0.044	50601.676	14.904	0.019	50601.672

Table 2—Continued

ID	V	σ_V	H.J.D. $_{V}$	B	σ_B	H.J.D. $_{B}$
			2,400,000+			2,400,000+
	13.312	0.012	51052.496	15.183	0.009	51052.492
V6	16.660	0.024	47213.902	17.515	0.023	47213.898
	16.474	0.030	47214.910	17.112	0.045	47214.910
	15.782	0.015	47215.906	16.228	0.014	47215.906
	16.458	0.035	47216.898	17.481	0.040	47216.895
	16.138	0.015	47217.906	16.754	0.024	47217.906
	16.529	0.039	47218.902	17.412	0.021	47218.902
	15.978	0.021	47220.898	16.574	0.014	47220.898
	16.517	0.031	47221.902	17.298	0.018	47221.902
	16.090	0.015	47222.910	16.671	0.013	47222.910
	16.672	0.028	48058.641	17.399	0.014	48058.629
	16.617	0.037	50601.676	17.372	0.038	50601.672
	16.672	0.025	51052.496	17.243	0.023	51052.492
V9	16.390	0.019	47213.902	16.972	0.018	47213.898
	15.835	0.025	47214.910	16.166	0.026	47214.910
	16.915	0.035	47215.906	17.881	0.043	47215.906
	16.837	0.029	47216.898	17.668	0.037	47216.895
	16.813	0.026	47217.906	17.570	0.055	47217.906
	16.403	0.020	47218.902	17.058	0.020	47218.902
	16.946	0.034	47220.898	17.931	0.043	47220.898
	16.836	0.028	47221.902	17.680	0.024	47221.902
	16.752	0.030	47222.910	17.688	0.039	47222.910
	16.632	0.016	48058.641	17.202	0.013	48058.629
	16.852	0.050	50601.676	17.452	0.043	50601.672
	16.480	0.027	51052.496	16.959	0.019	51052.492
V10	15.330	0.031	47213.902	16.537	0.013	47213.898
	15.276	0.044	47214.910	16.664	0.079	47214.910
	15.289	0.050	47215.906	16.696	0.065	47215.906
	15.306	0.053	47216.898	16.627	0.077	47216.895
	15.301	0.030	47217.906	16.598	0.049	47217.906
	15.300	0.047	47218.902	16.604	0.048	47218.902
	15.248	0.054	47220.898	16.701	0.066	47220.898
	15.271	0.063	47221.902	16.608	0.031	47221.902

Table 2—Continued

ID	<i>V</i>	σ_V	H.J.D. _{<i>V</i>} 2,400,000+	<i>B</i>	σ_B	H.J.D. _{<i>B</i>} 2,400,000+
V11	15.275	0.036	47222.910	16.825	0.066	47222.910
	16.558	0.020	47213.902	17.396	0.032	47213.898
	16.472	0.035	47214.910	17.189	0.045	47214.910
	15.825	0.016	47215.906	16.277	0.016	47215.906
	16.568	0.054	47216.898	17.407	0.040	47216.895
	16.432	0.051	47217.906	17.112	0.030	47217.906
	15.852	0.027	47218.902	16.339	0.018	47218.902
	16.313	0.049	47220.898	16.883	0.034	47220.898
	16.633	0.025	47221.902	17.240	0.027	47221.902
	16.583	0.036	47222.910	17.338	0.031	47222.910
V12	16.801	0.035	48058.641	17.552	0.028	48058.629
	16.221	0.056	50601.676	17.108	0.043	50601.672
	16.510	0.033	51052.496	17.319	0.041	51052.492
	14.519	0.005	47213.902	14.929	0.004	47213.898
	14.449	0.007	47214.910	14.850	0.014	47214.910
	14.502	0.007	47215.906	14.905	0.008	47215.906
	14.853	0.011	47216.898	15.356	0.009	47216.895
	14.892	0.011	47217.906	15.486	0.008	47217.906
	14.868	0.006	47218.902	15.429	0.007	47218.902
	14.518	0.011	47220.898	14.968	0.012	47220.898
V13	14.435	0.009	47221.902	14.863	0.007	47221.902
	14.480	0.007	47222.910	14.884	0.005	47222.910
	14.700	0.020	50601.676	15.152	0.023	50601.672
	14.639	0.011	51052.496	15.109	0.010	51052.492

Table 3. Summary of Light Curve Characteristics

ID	P (days)	A_B	A_V	$\langle B \rangle$	$\langle V \rangle$	$(B - V)_{\min}$	Type
V1	0.724704	1.20	0.95	17.29	16.60	0.75	RRab
V2	0.636044	1.60	1.05	17.12	16.37	1.00	RRab
V4	$\gtrsim 20$	0.3	0.2	13.26	15.01		Semiregular
V6	0.627247	1.60	1.15	17.23	16.46	0.80	RRab
V9	0.554631	2.00	1.40	17.54	16.72	0.90	RRab
V10	...	0.2	0.1	16.66	15.29		
V11	0.608155	1.50	1.20	17.22	16.47	0.80	RRab
V12	0.348834	0.70	0.50	15.15	14.66		foreground RRc